Reconstruction of Inhomogeneous Lossy Dielectric Objects in One Dimension

W. Rieger, M. Haas, C. Huber, G. Lehner and W.M. Rucker
Institut für Theorie der Elektrotechnik, Universität Stuttgart
Pfaffenwaldring 47, 70569 Stuttgart, Germany

***Abstract*— The 1D inverse scattering problem of reconstructing the material properties of an inhomogeneous lossy dielectric slab is considered. The material properties are reconstructed using scattering data from time harmonic electromagnetic plane waves. The incident plane waves are either TE or TM polarized. The inverse scattering problem formulated as a nonlinear optimization problem by means of integral equations is numerically solved using an iterative scheme and Tikhonov regularization. Numerical examples with both types of polarization are presented.**

I. Introduction

In this paper we consider the inverse scattering problem of reconstructing the permittivity and conductivity profile of an inhomogeneous lossy dielectric slab from the known incident and scattered electric fields.

The solution methods for both the direct and the inverse scattering problem are based on integral equations.

The medium of interest is probed by plane waves at a single frequency which are either TE or TM polarized. The waves are incident at a finite number of angles. The plane of incidence is assumed to be parallel to the $x-y$ plane. We define the TE waves to be linearly polarized with the electric field vector perpendicular to the plane of incidence, the TM waves to be linearly polarized with the electric field vector parallel to the plane of incidence. The inversion algorithm employs measurement data from either two receivers ($R1$ and $R2$) or from one receiver ($R1$), see Fig. 1.

All measurement data used for the inversion are simulated by numerically solving the corresponding direct scattering problem. The error level of the measurement data can be estimated to be $err < 5.0 \cdot 10^{-4}\%$. Hereby as in the following the relative mean square error defined by $err := \|\tilde{f} - f\|_{L_2} / \|f\|_{L_2}$ is used to specify a deviation of a disturbed function $\tilde{f}$ compared to its original f.

As the inverse electromagnetic scattering problem is nonlinear, an iterative scheme [5], [4] is applied to reduce the nonlinear problem to a sequence of linear integral equations which are severely *ill-posed* [2], [1]. To obtain stable approximate solutions to the *ill-posed* integral equations of the first kind, some kind of regularization is needed. In this paper Tikhonov regularization was applied. As the iterative algorithm starts with an initial estimate of the material properties the procedure allows to consider *a priori* information.

For the numerical evaluation of all integral operators we used the point-matching method with Gaussian quadrature. Quadratic isoparametric finite elements were used for the simulation of the measurement data. In order to rule out so called *inverse crimes* [1], different discretizations are used for the simulation of the measurement data and for the reconstruction of the material profile. Numerical examples show the performance of the inversion algorithm for both polarization types (TE and TM). In the case of TE polarization a wider range of contrasts could be reconstructed. The simulations point out that the inversion algorithm is band-limiting.

Manuscript received September 23, 1996.
W. Rieger, e-mail wolfgang.rieger@ite.uni-stuttgart.de

II. Direct Electromagnetic Scattering

An inhomogeneous lossy dielectric slab with thickness $l = x_2 - x_1$, embedded in free space, is successively illuminated by N time harmonic electromagnetic plane waves with either TE or TM polarization (see Fig. 1). The illuminated nonmagnetic material is described by

$$n(x) = \frac{1}{\varepsilon_0}[\varepsilon(x) + i\frac{\kappa(x)}{\omega}], \tag{1}$$

where $\varepsilon(x)$ denotes the permittivity, $\kappa(x)$ the conductivity and ω the angular frequency of the incident plane waves.

A. TE polarization

In the case of TE polarization we have N time harmonic incident plane waves

$$E_z^{inc} = E_z^i(x, \theta_r) \exp(ik_0 \sin\theta_r\, y) \exp(-i\omega t), \tag{2}$$

with wave number $k_0 = \omega\sqrt{\varepsilon_0\mu_0}$, angular frequency ω, angle of incidence θ_r, $r \in [1, N]$, and

$$E_z^i(x, \theta_r) = E_0 \exp(ik_0 \cos\theta_r\, x). \tag{3}$$

Using

$$E_z^{tot} = E_z(x, \theta_r) \exp(ik_0 \sin\theta_r\, y) \exp(-i\omega t) \tag{4}$$

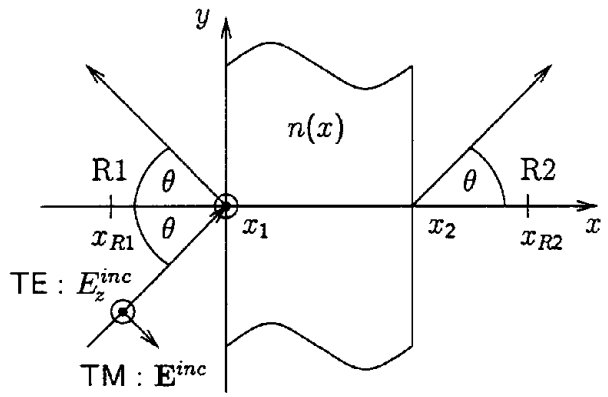

Fig. 1. Geometrical configuration of the problem

for the total field, the underlying differential equation reads [3]

$$\left(\frac{\mathrm{d}^2}{\mathrm{d}x^2} + k_0^2\left[n(x) - \sin^2\theta_r\right]\right) E_z(x,\theta_r) = 0, \qquad (5)$$

where $x \in [x_1, x_2]$. The second kind integral equation

$$\begin{aligned} E_z(x,\theta_r) &= E_z^i(x,\theta_r) + E_z^s(x,\theta_r) \\ &= E_z^i(x,\theta_r) - k_0^2 \int_{x_1}^{x_2} m(x') G(x,x',\theta_r) E_z(x',\theta_r)\,\mathrm{d}x' \end{aligned} \qquad (6)$$

holds for $E_z(x,\theta_r)$, $x \in \mathbb{R}$, where

$$m(x') = 1 - n(x') \qquad (7)$$

and

$$G(x,x',\theta_r) = \frac{i}{2k_0\cos\theta_r} \exp(ik_0\cos\theta_r\,|x-x'|) \qquad (8)$$

denotes Green's function.

B. TM polarization

In this case the N time harmonic incident plane waves take the form

$$\mathbf{E}^{inc} = \mathbf{E}^i(x,\theta_r)\exp(ik_0\sin\theta_r\,y)\exp(-i\omega t), \qquad (9)$$

where

$$\mathbf{E}^i(x,\theta_r) = E_0 \begin{bmatrix} \sin\theta_r \\ -\cos\theta_r \end{bmatrix} \exp(ik_0\cos\theta_r\,x). \qquad (10)$$

The total electric field $\mathbf{E}^{tot}$ can be written as

$$\mathbf{E}^{tot} = \mathbf{E}^*(x,y,\theta_r)\exp(-i\omega t), \qquad (11)$$

where $\mathbf{E}^*(x,y,\theta_r) = \mathbf{E}(x,\theta_r)\exp(ik_0\sin\theta_r\,y)$. Using (11), the wave equation reads [3]

$$\operatorname{curl}\operatorname{curl}\mathbf{E}^* - k_0^2 n(x)\mathbf{E}^* = 0, \qquad x \in [x_1, x_2]. \qquad (12)$$

As solution to (12), we obtain for $\mathbf{E}(x,\theta_r)$, $x \in [x_1,x_2]$, a second kind integral equation

$$\begin{aligned} &\begin{bmatrix} n(x) & 0 \\ 0 & 1 \end{bmatrix} \mathbf{E}(x,\theta_r) = \mathbf{E}^i(x,\theta_r) \\ &- k_0^2 \int_{x_1}^{x_2} m(x')\overline{\overline{G}}(x,x',\theta_r)\mathbf{E}(x',\theta_r)\,\mathrm{d}x', \end{aligned} \qquad (13)$$

where $\overline{\overline{G}}(x,x',\theta_r)$ denotes a second rank tensor

$$\overline{\overline{G}}(x,x',\theta_r) = \begin{pmatrix} G\sin^2\theta_r & -\frac{i}{k_0}\sin\theta_r\frac{\mathrm{d}G}{\mathrm{d}x'} \\ -\frac{i}{k_0}\sin\theta_r\frac{\mathrm{d}G}{\mathrm{d}x'} & G\cos^2\theta_r \end{pmatrix}, \qquad (14)$$

and G is known from (8).
Outside the material, $x \notin [x_1,x_2]$, there is $n(x) = 1$ and $\mathbf{E}(x,\theta_r)$, $x \notin [x_1,x_2]$, is obtained from

$$\begin{aligned} \mathbf{E}(x,\theta_r) &= \mathbf{E}^i(x,\theta_r) + \mathbf{E}^s(x,\theta_r) \\ &= \mathbf{E}^i(x,\theta_r) - k_0^2 \int_{x_1}^{x_2} m(x')\overline{\overline{G}}(x,x',\theta_r)\mathbf{E}(x',\theta_r)\,\mathrm{d}x', \end{aligned} \qquad (15)$$

using the solution of (13).

III. The Reconstruction Method

For each incident field the components of the scattered electric field are collected at M points x_{Rj}, $x_{Rj} \notin [x_1,x_2]$, $j \in [1,M]$, where $M = 2$ in the case of two receivers and $M = 1$ if one receiver is used. Given the measured scattered electric field $\hat{E}_z^s(x_{Rj},\theta_r)$ in the TE case, the first kind integral equation

$$\hat{E}_z^s(x_{Rj},\theta_r) = -k_0^2 \int_{x_1}^{x_2} m(x')G(x_{Rj},x',\theta_r)E_z(x',\theta_r)\,\mathrm{d}x' \qquad (16)$$

has to be solved for m. In the TM case the first kind integral equation

$$\hat{\mathbf{E}}^s(x_{Rj},\theta_r) = -k_0^2 \int_{x_1}^{x_2} m(x')\overline{\overline{G}}(x_{Rj},x',\theta_r)\mathbf{E}(x',\theta_r)\,\mathrm{d}x' \qquad (17)$$

relates the measured scattered electric field $\hat{\mathbf{E}}^s(x_{Rj},\theta_r)$ with m and $\mathbf{E}$. As the electric field E_z in (16) and $\mathbf{E}$ in (17) also depends on m via (6) or (13), respectively, the inverse electromagnetic scattering problem is nonlinear. Due to the smoothness of G and $\overline{\overline{G}}$, (16) and (17) are severely *ill-posed* and some kind of regularization is needed to obtain a stable approximate solution [1].

Applying an iterative procedure, the nonlinear relations (16), (17) can be replaced by a sequence of linear ones.

The iterative algorithm starts with an initial estimate of n, which allows to consider *a priori* information. The iterative approach can be summarized in the following steps:

1. Solve the direct scattering problem (6), (13) for the field inside the medium, and (6), (15) for the field at the observation points using the last reconstructed material properties.
2. Substitute the fields ($x \in [x_1, x_2]$) obtained from step 1 into (16) or (17), respectively, and solve the inverse medium problem to recover the next permittivity and conductivity profile by using Tikhonov regularization with a certain regularization parameter.
3. Repeat step 1 and compare the field, calculated at the observation points using the reconstructed profile of step 2, with the measured field data. If the difference is less than a certain bound, adopt the last regularization parameter, otherwise determine a new regularization parameter. Repeat step 2 - 3 until the solution converges.

The point-matching method is used to solve the direct and the inverse scattering problem in this inversion algorithm. For the discretization of the electric field and the material properties, we use a finite element approximation with the pulse functions $N_p(x)$ as basis functions. Using the basis functions $N_p(x)$, $m(x)$ can be written as

$$m(x) = \sum_{p=1}^{P} N_p(x) m_p, \tag{18}$$

where m_p is the value of $m(x)$ at the center of the pth finite element. The parameter P represents the number of finite elements. Substituting (18) in (16) or in (17), respectively, and collecting $\hat{E}_z^s(x_{Rj}, \theta_r)$ or $\hat{\mathbf{E}}^s(x_{Rj}, \theta_r)$ for each angle of incidence and at each observation point, we obtain the following linear algebraic representation

$$[A]\{m\} = \{b\}. \tag{19}$$

In the case of TE polarization $[A]$ is a $(N \cdot M) \times P$ matrix whose elements are

$$A_{lp} = -k_0^2 \int_{S_p} G(x_{Rj}, x', \theta_r) E_z(x', \theta_r) N_p(x') \, \mathrm{d}x', \tag{20}$$

where S_p is the domain of the pulse function N_p, $p \in [1, P]$ and $l \in [N \cdot M]$. The vector $\{b\}$ contains the measured fields

$$\{b\} = [\hat{E}_z^s(x_{R1}, \theta_1), ..., \hat{E}_z^s(x_{R2}, \theta_N)]^T, \tag{21}$$

while the vector $\{m\}$ consists of the values m_p

$$\{m\} = [m_1, ..., m_P]^T. \tag{22}$$

In the case of TM polarization $[A]$ is a $(2 \cdot N \cdot M) \times P$ matrix due to the vectorial formulation. The matrix elements are constructed in a similar manner to the TE case.

IV. Regularization and Parameter Choice

Equation (19) represents an ill-conditioned linear system. Therefore a regularization procedure has to be employed to stabilize the results. Instead of solving (19), the Tikhonov functional

$$F(\{m\}) = \|[A]\{m\} - \{b\}\|^2 + \alpha \|\{m\}\|^2 \tag{23}$$

is minimized [1], where α is the regularization parameter. The unique solution $\{m\}$ of (23) depending on the parameter α is given by

$$\{m\} = ([A]^*[A] + \alpha [I])^{-1} [A]^* \{b\}, \tag{24}$$

where $[A]^*$ denotes the conjugate transpose of $[A]$ and [I] is the identity matrix. The choice of the parameter α is crucial to the convergence of the iterative scheme. A small parameter α puts more weight on minimizing the first term in (23) and emphasizes the accuracy between the computed and the measured field at the observation points. A large parameter α stresses the second term in (23) and cares for a stable solution. The choice of the parameter α is a kind of compromise between accuracy and stability.

The initial iteration steps result in relative large errors between the calculated and the measured data at the observation points. For that reason emphasis should be taken on minimizing the second term in (23), corresponding to larger values of α. As the iteration processes, $\{m\}$ approaches the true profile. Hence more weight should be put on the first term in (23), corresponding with a smaller α. Starting with an initial regularization parameter α_0, the parameter α is decreased at each iteration step, until the error $err_{s,i}$ between computed and measured electric field at the observation points is below a certain limit e. The error $err_{s,i}$ between computed and measured electric field at the receivers is defined by

$$err_{s,i} = \left[\frac{\sum_{l=1}^{N \cdot M} |b_{l,i} - b_l|^2}{\sum_{l=1}^{N \cdot M} |b_l|^2} \right]^{\frac{1}{2}}. \tag{25}$$

Hereby $b_{l,i}$ denotes the lth component of the computed field at the ith iteration step, b_l the lth component of the measured field at the receiver locations in correspondance to (21).

We choose the regularization parameter α to be

$$\alpha_{i+1} = \beta \, \alpha_i, \tag{26}$$

where the reduction factor $\beta \in (0, 1)$ is determined empirically and i denotes the iteration step. In order to avoid too small parameters which result in unstable solutions the reduction factor β is set to $\beta = 1$ if the error $err_{s,i}$ is less than a certain prespecified limit e. The resulting regularization parameter is employed until the iteration converges.

V. Numerical Results

In all examples presented in this paper, the profile was reconstructed from simulated data. For the simulation of the measurement data, we used a finite element mesh with 80 quadratic isoparametric finite elements, and the scattered electric fields were calculated at the two receivers $R1$ and $R2$ at $x_{R1} = -0.2$ m and $x_{R2} = 1.2$ m in all examples. The thickness l of the slab was chosen $l = 1$ m. In order to rule out so called *inverse crimes* [1], different discretizations were used for the simulation of the measurement data and for the inverse scattering problem. Therefore we used a finite element mesh with $P = 50$ constant elements in the inversion procedure, where the electric field, the permittivity and the conductivity are assumed to be constant. The relative mean square error of the reconstructed profile at the ith iteration step is defined as

$$err_{m,i} = \left[\frac{\sum_{p=1}^{P} |m_{p,i} - m_p|^2}{\sum_{p=1}^{P} |m_p|^2} \right]^{\frac{1}{2}}, \qquad (27)$$

where p, m_p and $m_{p,i}$ denote, respectively, the finite element number, the exact values of the function $m(x)$ and the reconstructed values of $m(x)$ at the ith iteration step at the center of the pth finite element.

In all examples we chose the initial regularization parameter $\alpha_0 = 0.01$ and the reduction factor $\beta = 0.5$. All examples were reconstructed knowing the boundary of the slab *a priori*. The iteration scheme started in each case by the initial estimate $n(x) = 1$. Numerical simulations show that the convergence of the inversion algorithm could be accelerated by using *a priori* information about $n(x)$. Unless explicitly mentioned, in all examples the reconstructions were calculated using measurement data from both receivers. The angles of incidence θ_r are equally spaced in the range $[0°, 70°]$ for the N incident plane waves in all examples.

A. TE polarization

Fig. 2 and Fig. 3 show the reconstruction of the profile $n(x) = 1 - m(x) = 1 + \sin(\pi x/l) + i\sin(\pi x/l)$, where the error of reconstruction is 3.5% with a proposed error bound of $e = 10^{-1}\%$. We used $N = 70$ incident plane waves at an operating frequency of $f = \omega/2\pi = 50$ MHz. The wave length λ in free space is $\lambda = 6$ m.

The numerical convergence of the profile error $err_{m,i}$ and the error $err_{s,i}$ is plotted in Fig. 4 and in Fig. 5, where the proposed bound e to stop the reduction of the regularization parameter α is varied. The results clearly show that the reconstructions depend on this error limit. If the bound e is selected too small, e.g. $e = 10^{-4}\%$, the inversion algorithm doesn't converge and we obtain an unstable solution without any physical meaning.

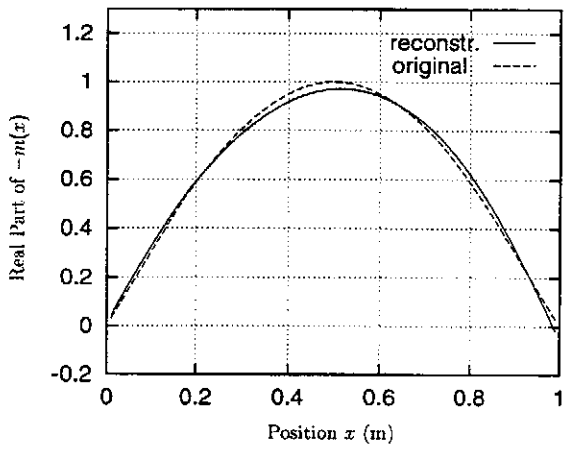

Fig. 2. Reconstruction of the real part of $-m(x)$ compared to the original; the profile is described by $n(x) = 1+\sin(\pi x/l)+i\sin(\pi x/l)$; the error of reconstruction is 3.5% ($e = 10^{-1}\%$).

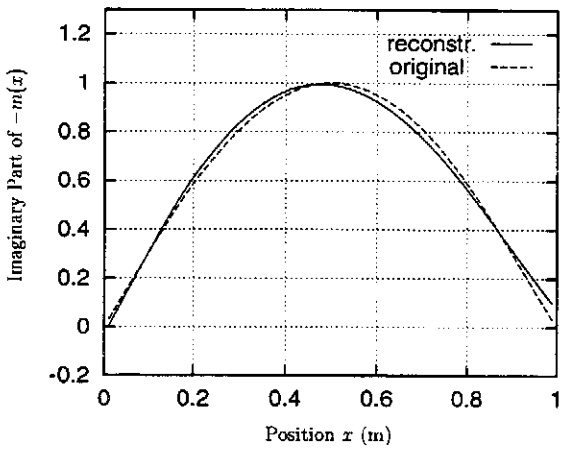

Fig. 3. Reconstruction of the imaginary part of $-m(x)$ compared to the original; the profile is described by $n(x) = 1 + \sin(\pi x/l) + i\sin(\pi x/l)$.

Table I lists the reconstruction errors obtained by varying the error limit e.

TABLE I
Error Bounds And Reconstruction Errors

e	$10^{-1}\%$	$10^{-2}\%$	$10^{-3}\%$	$10^{-4}\%$
$err_{m,i}$	3.5%	1.8%	0.8%	failed

Reconstruction errors corresponding to different error bounds e for the profile $n(x) = 1 + \sin(\pi x/l) + i\sin(\pi x/l)$.

As in practice the profile error $err_{m,i}$ cannot be measured, the only available measure of convergence is the error quantity $err_{s,i}$.

Reconstructing the profile only with measurement data from one receiver at x_{R1} leads to a reconstruction error of 10.3% with $e = 10^{-1}\%$ and to a reconstruction error of 4.7% with $e = 4 \cdot 10^{-2}\%$. The reconstruction failed for $e = 10^{-2}\%$. The numerical examples show, that better results are obtained by using data from both receivers.

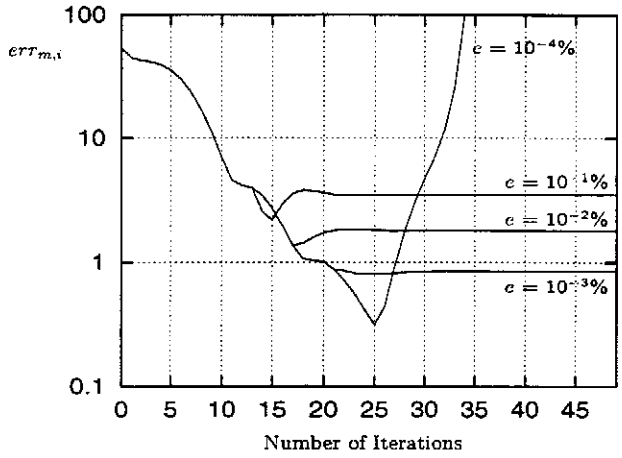

Fig. 4. Reconstruction error $err_{m,i}$ in % versus the number of iterations for different error bounds e.

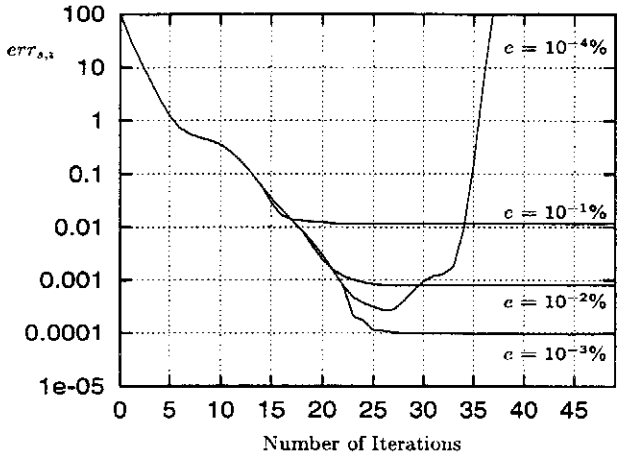

Fig. 5. Error $err_{s,i}$ in % between the computed and the measured field at the observation points versus the number of iterations for different error bounds e.

The results of the reconstruction of a more complicated profile $n(x) = 1 - m(x) = 2 + (x/l)\sin(2\pi x/l) + i\sin(\pi x/l)$ are plotted in Fig. 6 and Fig. 7. Again we used 70 plane waves at an operating frequency of $f = 50$ MHz. The reconstruction yields an error of 3.1% with an error bound $e = 2 \cdot 10^{-3}\%$.

In the next example we consider an object with discontinuous profile

$$n(x) = 1 - m(x) = \begin{cases} 2.00 + i\,(x/l)^2, & x/l \in [0.0, 0.5] \\ 1.25 + i\,(x/l)^2, & x/l \in (0.5, 1.0] \end{cases}.$$

The measurement data were simulated using 70 incident plane waves at an operating frequency of $f = 100$ MHz. The error limit e was chosen $e = 10^{-1}\%$. Fig. 8 and Fig. 9 show the results of the reconstruction. The inversion algorithm is band-limiting and we obtain a smoothed version of the profile. Additional numerical simulations confirmed that our inversion algorithm reconstructs smooth profiles very accurately, while for discontinuous profiles band-limited reconstructions are obtained.

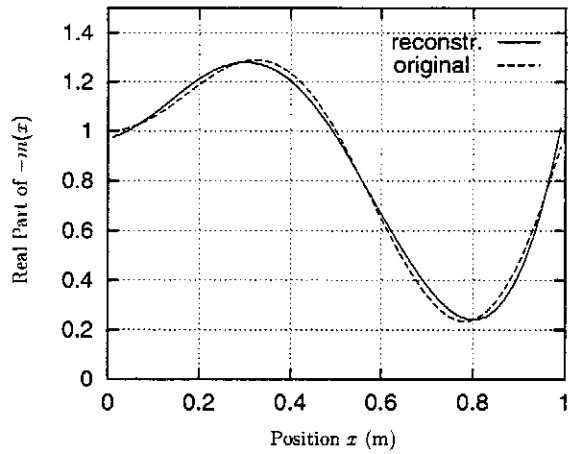

Fig. 6. Reconstruction of the real part of $-m(x)$ compared to the original; the profile is described by $n(x) = 2 + (x/l)\sin(2\pi x/l) + i\sin(\pi x/l)$; the error of reconstruction is 3.1% ($e = 2 \cdot 10^{-3}\%$).

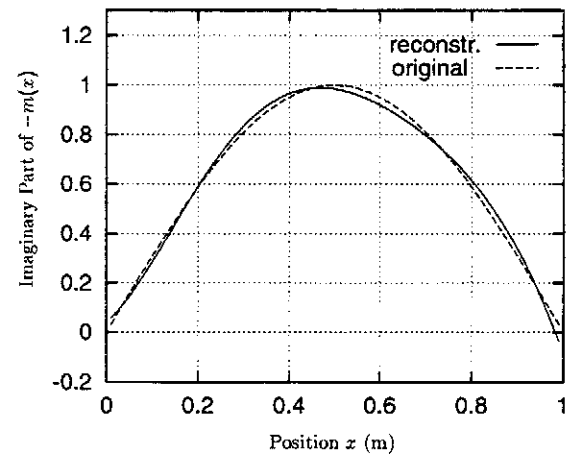

Fig. 7. Reconstruction of the imaginary part of $-m(x)$ compared to the original; the profile is described by $n(x) = 2 + (x/l)\sin(2\pi x/l) + i\sin(\pi x/l)$.

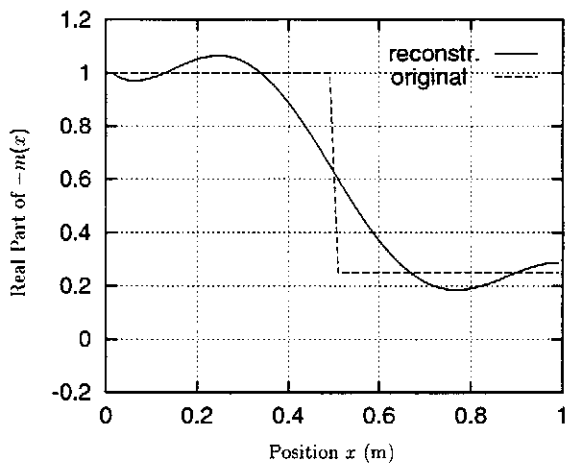

Fig. 8. Reconstruction of the real part of $-m(x)$ compared to the original; discontinuous profile.

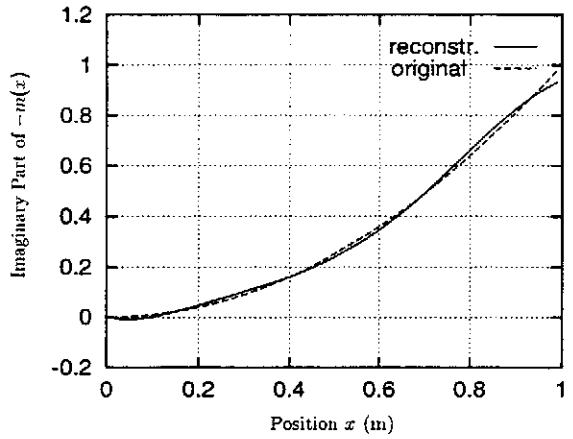

Fig. 9. Reconstruction of the imaginary part of $-m(x)$ compared to the original; discontinuous profile.

B. TM polarization

Fig. 10 and Fig. 11 show the reconstruction of the profile $n(x) = 1 - m(x) = 1.0 + 0.5\sin(\pi x/l) + 0.5\,i\,\sin(\pi x/l)$. We used 50 incident plane waves at an operating frequency of $f = 100$ MHz. Table II shows a comparison of the achieved reconstruction errors in the TE and the TM case corresponding to different error bounds e using the same parameter configuration in both polarization cases.

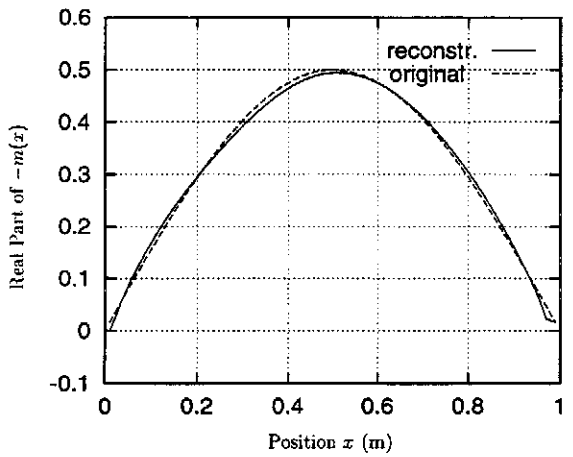

Fig. 10. Reconstruction of the real part of $-m(x)$ compared to the original; the profile is described by $n(x) = 1.0 + 0.5\sin(\pi x/l) + 0.5\,i\sin(\pi x/l)$; the error of reconstruction is 3.2% ($e = 10^{-1}\%$).

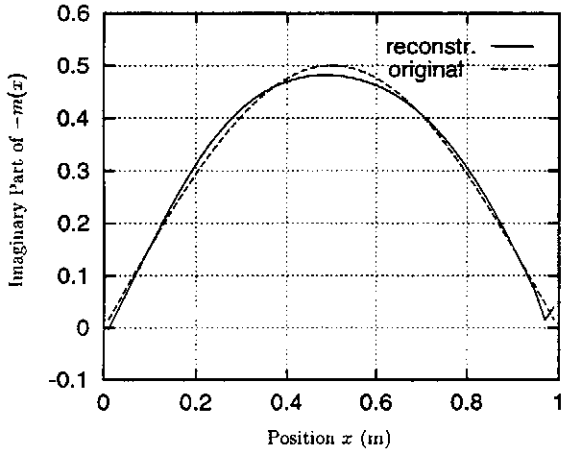

Fig. 11. Reconstruction of the imaginary part of $-m(x)$ compared to the original; the profile is described by $n(x) = 1.0 + 0.5\sin(\pi x/l) + 0.5\,i\sin(\pi x/l)$.

TABLE II
ERROR BOUNDS AND RECONSTRUCTION ERRORS

e	$10^{-1}\%$	$5\cdot10^{-2}\%$	$10^{-2}\%$	$10^{-3}\%$	$5\cdot10^{-4}\%$
$TM: err_{m,i}$	3.2%	1.3%	failed	–	–
$TE: err_{m,i}$	5.0%	3.7%	1.7%	1.4%	failed

Comparison of reconstruction errors corresponding to different error bounds e for the profile $n(x) = 1 + 0.5\sin(\pi x/l) + 0.5i\sin(\pi x/l)$ in TE and in TM case.

Comparing the reconstructions obtained by TE polarized incident waves to the results of TM polarized waves, a wider range of profiles could be reconstructed in the case of TE polarization. Using TM polarized incident waves the reconstructions succeeded as long as the deviation of $n(x)$ from the mean value of $n(x)$ was not too large. The influence of a combination of both polarization types on the reconstruction of material profiles has still to be explored.

VI. CONCLUSION

A numerical method for solving the 1D nonlinear inverse electromagnetic scattering problem based on integral equations has been proposed using TM or TE polarized probing waves.

Several examples have been investigated. From the above results one can conclude that the algorithm gives reasonable reconstructions of smoothly varying permittivity and conductivity profiles.

In the case of discontinuous profiles, the method leads to a smoothed i.e. to a filtered version of the profile.

The numerical simulations show that in the case of TE polarization the range of the profiles the inversion algorithm is able to reconstruct is larger than in the TM case.

REFERENCES

[1] Colton, D. and Kress, R. *Inverse Acoustic and Electromagnetic Scattering Theory.* Applied Mathematical Sciences 93. Springer, Berlin Heidelberg New York, 1992.

[2] Kress, R. *Linear Integral Equations.* Applied Mathematical Sciences 82. Springer, Berlin Heidelberg New York, 1989.

[3] Lehner, G. *Elektromagnetische Feldtheorie für Ingenieure und Physiker.* Springer, Berlin Heidelberg New York, 3rd edition, 1996.

[4] Roger, A., Maystre D. and Cadilhac M. On a problem of inverse scattering in optics: The dielectric inhomogeneous medium. *Journal Optics*, **9**:83–90, 1978.

[5] Wang, Y. M., Chew, W. C. An iterative solution of the two-dimensional electromagnetic inverse scattering problem. *International Journal of Imaging Systems and Technology*, **1**:100–108, 1989.